Mon. Not. R. astr. Soc. (1983) **204**, 273–287

Spectrophotometry in the galactic supernova remnants RCW 86, 103 and Kepler

Elia M. Leibowitz* *Department of Physics and Astronomy and the Wise Observatory, Tel Aviv University, Israel*

I. J. Danziger *European Southern Observatory, Karl-Schwarzschild-Str. 2, 8046 Garching, West Germany*

Received 1982 October 14; in original form 1982 May 12

Summary. The results of spectrophotometric observations in the Galactic supernova remnants (SNR) RCW 86, 103 and Kepler are presented. The measurements were made with an angular resolution of about 4 arcsec in a number of different positions in each object. We also present the integrated spectra of the three remnants and compare them with the spectra of other Galactic SNRs. The differential measurements reveal variations from point to point in the extinction towards the three objects, as well as in their intrinsic relative line-intensities. Some implications of the observed variations are discussed in the context of abundances and shock conditions.

1 Introduction

Many spectrophotometric studies of supernova remnants have been carried out in the last few years (e.g. Miller 1974; Kirshner & Chevalier 1977; Fesen & Kirshner 1980; Blair, Kirshner & Chevalier 1981; Dopita, Mathewson & Ford 1977; D'Odorico & Sabbadin 1977). Those of extragalactic objects measure the spectrum of an entire optical remnant or of a large fraction of it, although it is clear that much information about an SNR is lost when the remnant is not resolved spatially. Even a simple inspection of direct photographs of SNRs, for example those by van den Bergh, Marscher & Terzian (1973), reveals the extreme patchiness of some optical nebulae. Spectroscopy of Vela by Danziger & Dennefeld (1976) and Cygnus by Miller (1974) also revealed large variations of relative line-strengths. Spectrophotometry at high angular resolution enables one in principle to study the variations of the physical conditions in these objects. Theoretical models make specific predictions about scale sizes for variation of the line-emitting regions, both optical and X-ray (see, for example, McKee & Cowie 1975; Bychkov & Pikel'ner 1975). The integrated light from an entire SNR is a superposition of emission from filaments that differ considerably in their physical and dynamical conditions, so the integrated spectrum cannot provide a data base for *critical* tests of models in which the fits of the theories to the observations are approaching the level of accuracy attainable by the observations.

* Visiting Associate, ESO.

In some Galactic SNRs the observational angular resolution now possible corresponds to a linear dimension at the remnant close to that estimated for a single filament. While a zone in the nebula with such a two-dimensional extension is still far from the ideal filament, because of the lack of resolution in the radial direction, the unknown geometry and the interaction with neighbouring hot filaments, it is nevertheless closer to the model than the whole nebula. One of us (JD) has initiated a program of spectroscopic observations at high spatial resolution in SNRs. Here we report the results of the observations in three Galactic sources, RCW 86, 103 and Kepler's SNR.

2 Observations

The spectra forming the basis of this study were obtained with the image-dissector-scanner attached to the Boller and Chivens spectrograph at the Cassegrain focus of the 3.9-m Anglo-Australian telescope. Our spectra have a nominal dispersion of 170 Å mm^{-1} and an effective resolution of about 10 Å, the entrance aperture being 3.5×3.5 $arcsec^2$. Flux calibration was achieved by observing white-dwarf standards (Oke 1974) on the same night through the same aperture. A standard atmospheric extinction curve was assumed.

The line strengths, especially involving the deconvolution of blended lines, were measured with a program developed at ESO and based on the CERN MINUIT program. This allowed multiple least-squares fitting of a linear combination of a Gaussian and a Cauchy function to data containing a maximum of five lines. Such a combination of functions was necessary to fit the non-Gaussian instrumental wings in the emission lines. The error in the line-fitting was estimated by varying the parameters of the fitted profile (e.g. the ratio of the widths of the Gaussian and the Cauchy components, the positions of the centres of the lines in the blend, etc) and observing the dependence of the inferred line-intensities on them. Some indication of the accuracy of our de-blending can be obtained by inspecting the line ratios 6584/6548 of [N II], given in Tables 1, 2 and 3. The two [N II] lines are blended in all our spectra with Hα, particularly the λ 6548 line. Nevertheless the line ratio in each case takes, within a few per cent, the expected value of 3, without assigning this value to the blend *a priori*. We estimate the error in the relative intensity of lines with $I \geqslant 100$ [on a scale where $I(\mathrm{H}\beta) = 100$] as $\leqslant 10$ per cent. The probable error increases up to 20 per cent for lines with $I \leqslant 30$. Because there is a drop in the signal-to-noise ratio of our detector at both ends of the spectral range, the intensities of all lines with $\lambda > 6800$ or $\lambda < 4000$ are accurate to no better than 50 per cent. In some individual lines, the uncertainty reaches 100 per cent. They are marked in the tables with brackets. The estimated error in the measured Hβ flux is 10 per cent.

3 Results

As examples, Figs 1, 2 and 3 are intensity tracings of the spectra of one of the brightest knots in each of our three objects. The spectral resolution in the original data is better than that seen in the figures, where the wavelength scale is compressed.

The main observational results are presented in Tables 1, 2 and 3. In each table the emission-line intensities for the different positions indicated in Plates 1, 2 and 3 are given relative to $I(\mathrm{H}\beta) = 100$; they have been corrected for interstellar reddening as described in Section 4. For each position we give the value of c – the reddening parameter, i.e. the logarithm of the extinction at Hβ. The original results, namely the observed intensities outside the Earth's atmosphere, can be reconstructed by applying the formula $\log I^{\circ}(\lambda) = \log I(\lambda) - cf(\lambda)$, where $I^{\circ}(\lambda)$ and $I(\lambda)$ are the observed and the corrected relative intensities

RCW 86

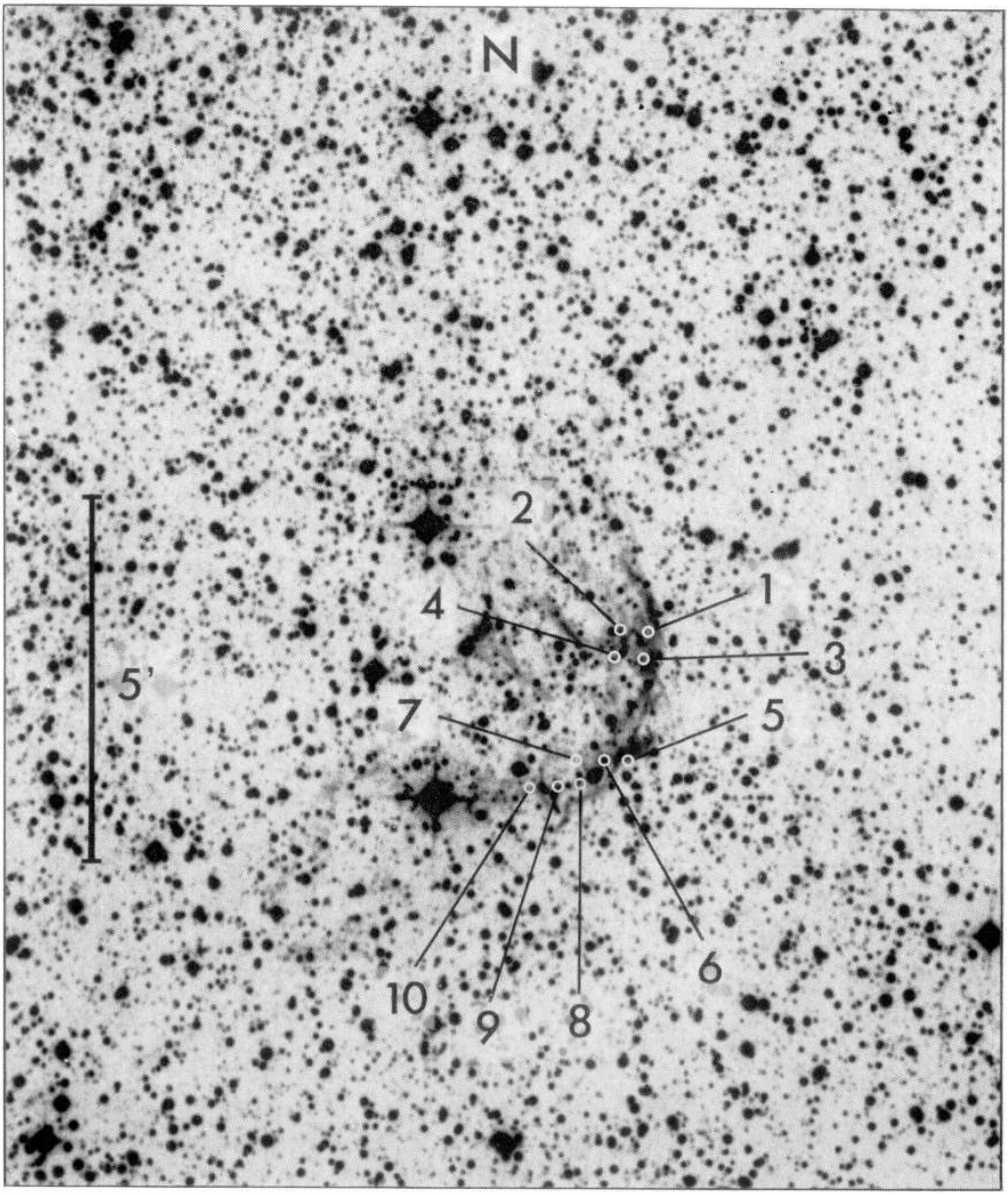

Plate 1. Direct plate of RCW 86 showing positions of the aperture. North is at the top and east on the left.

[*facing page* 274]

RCW 103

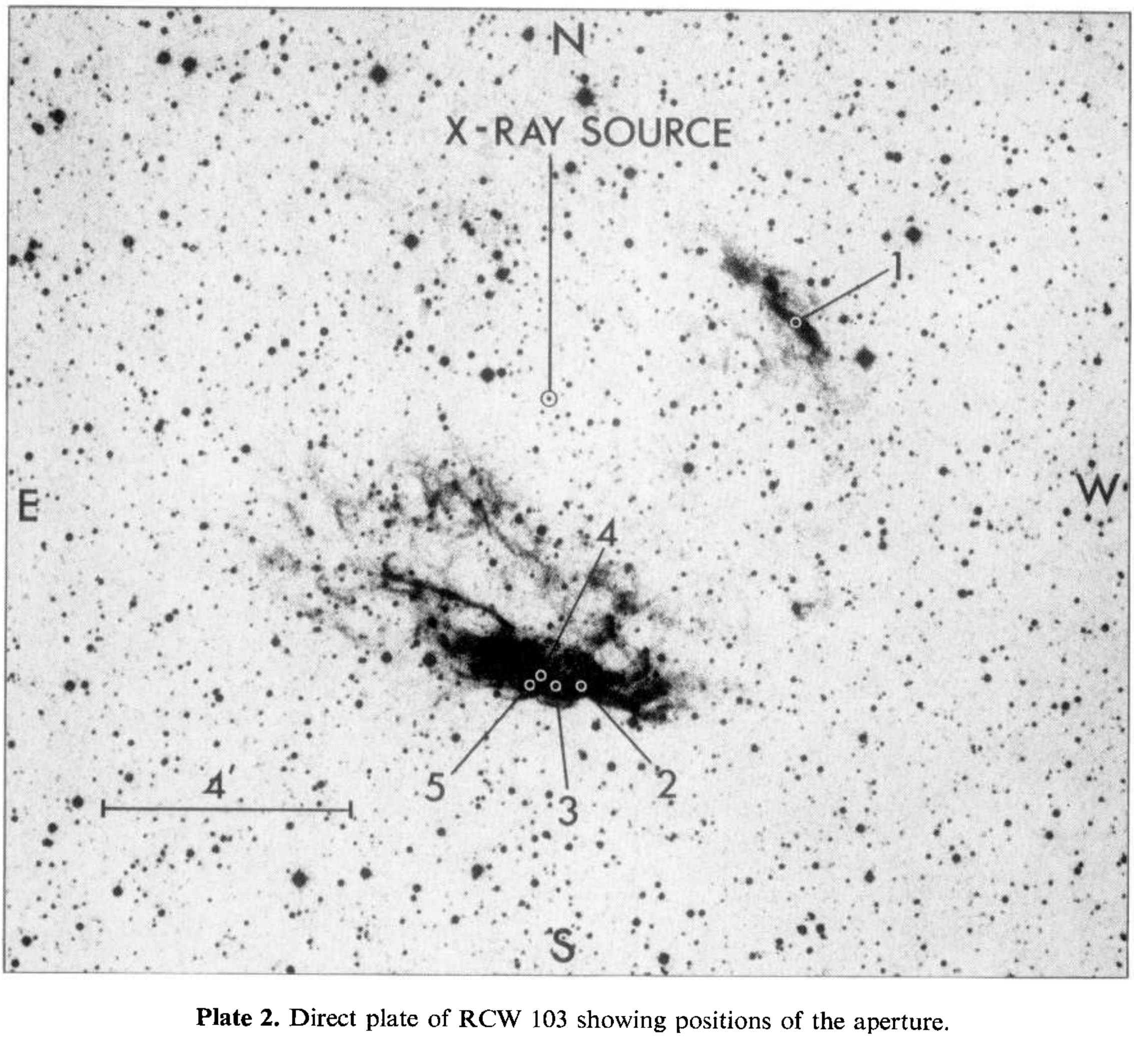

Plate 2. Direct plate of RCW 103 showing positions of the aperture.

1983MNRAS.204..273L

KEPLER

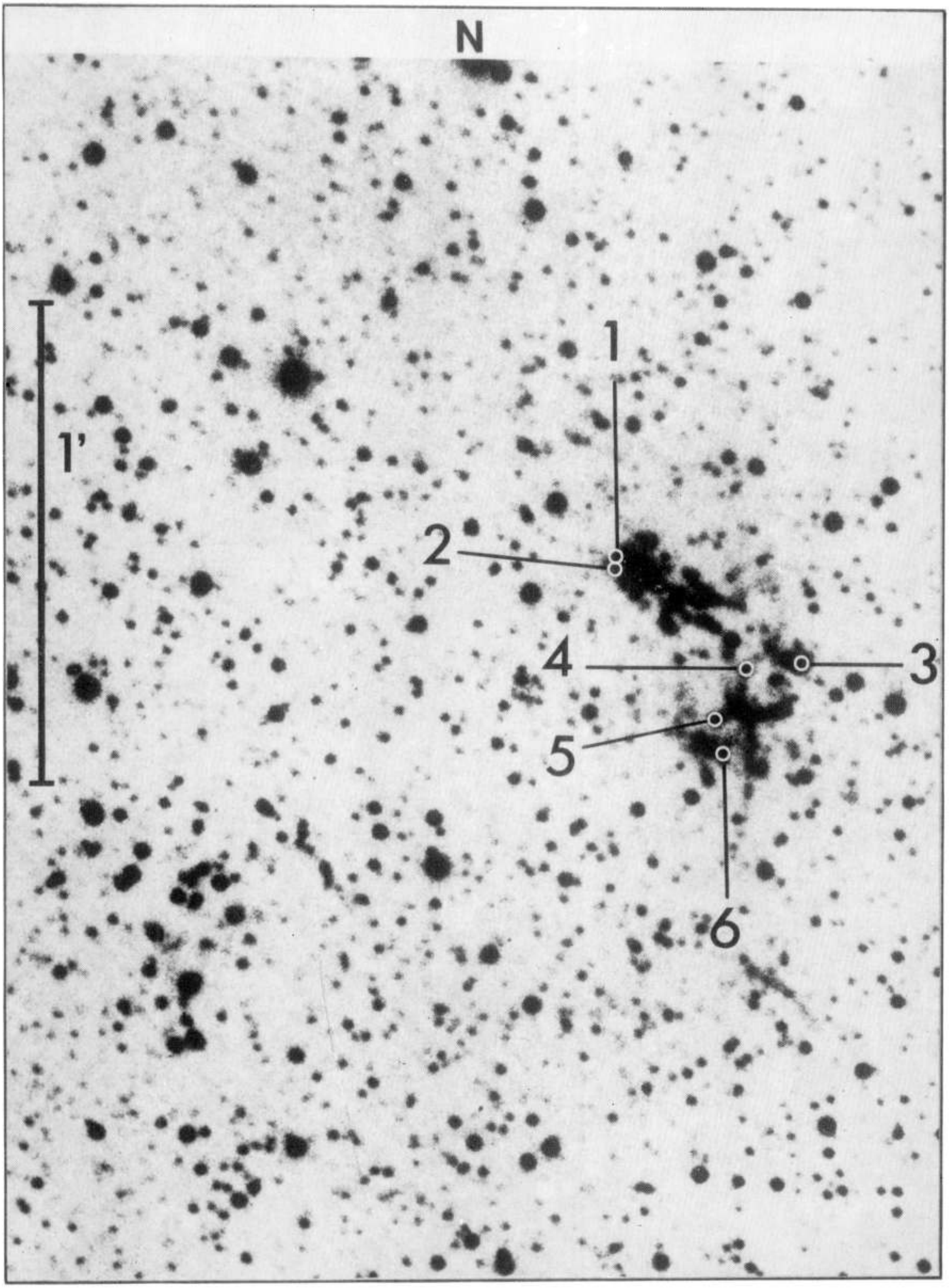

Plate 3. Reproduction of photograph of Kepler (van den Bergh *et al.* 1973) showing positions of the aperture. North is at the top and east on the left.

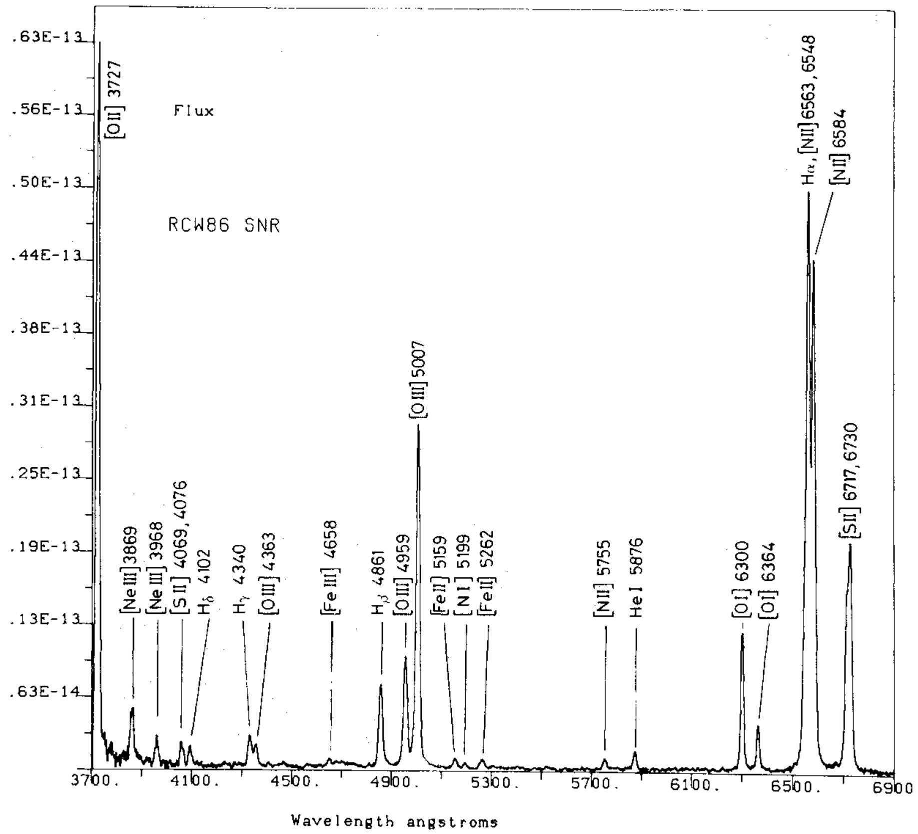

Figure 1. Spectrum of brightest filament in RCW 86 calibrated in wavelength units (erg cm^{-2} s^{-1} Å^{-1}).

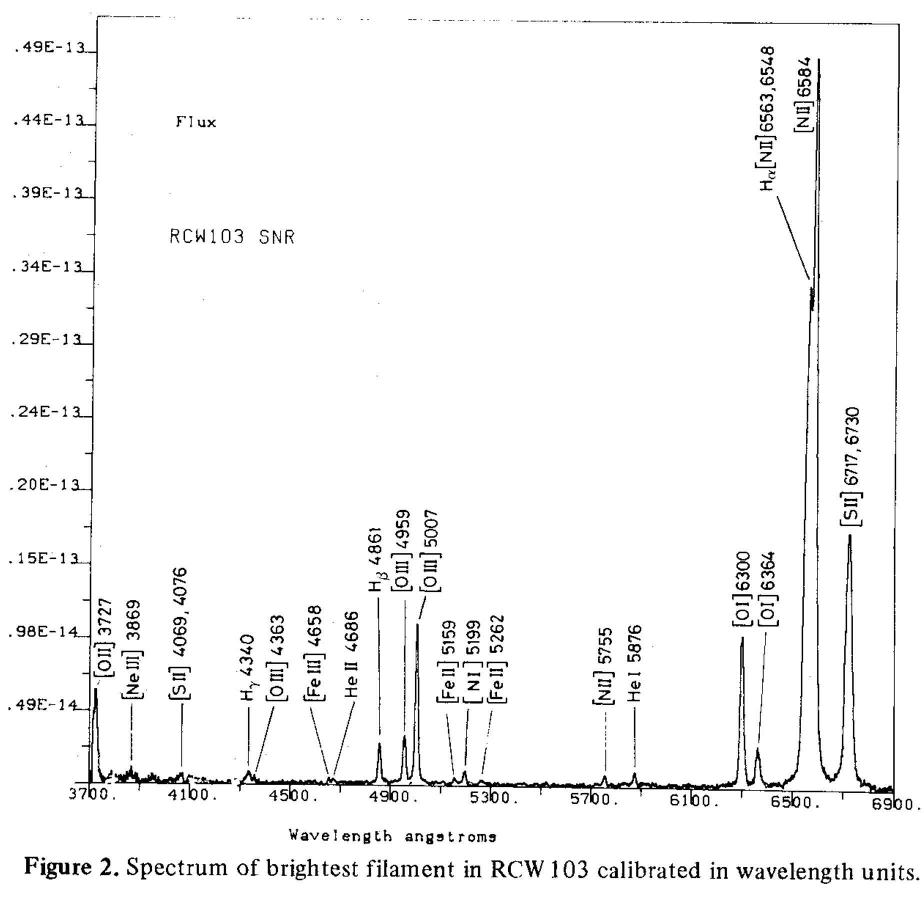

Figure 2. Spectrum of brightest filament in RCW 103 calibrated in wavelength units.

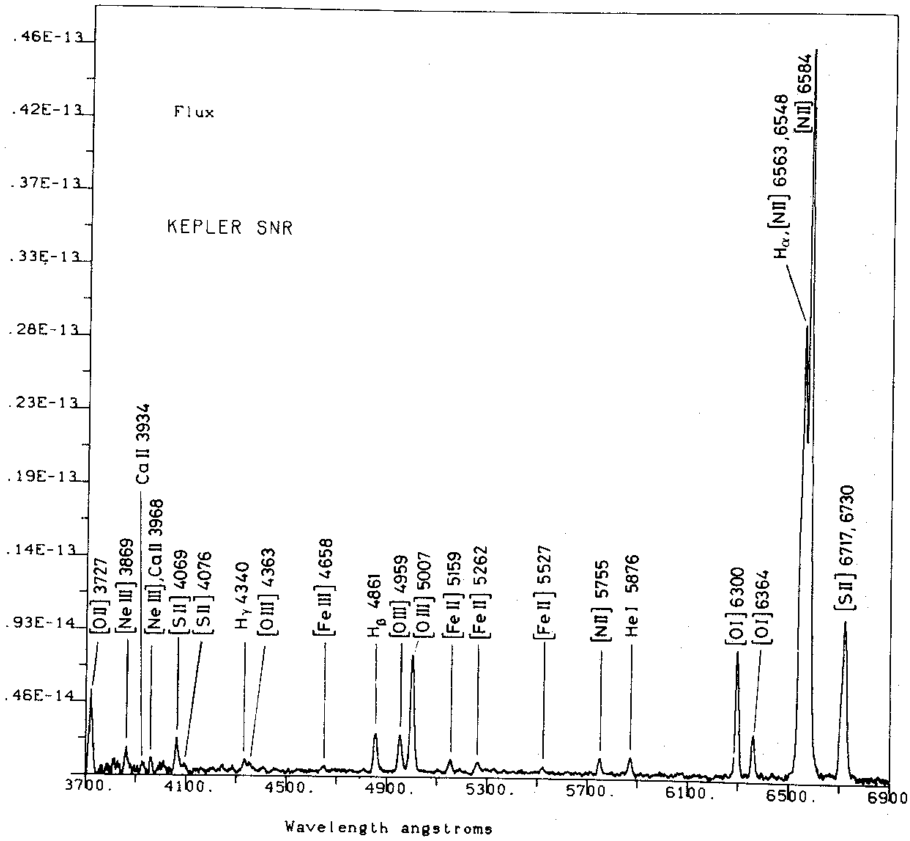

Figure 3. Spectrum of brightest filaments in Kepler calibrated in wavelength units.

Table 1. Dereddened emission line intensities for 10 positions in the SNR RCW 86.

		1	2	3	4	5	6	7	8	9	10
[Ne III]	3869					44	33				
He$^+$ [Ne III]	3970					49		(36)			
[S II]	4064					25	37	} 62		43	
[S II]	4076					39					
Hδ	4102	78				26	28	(35)		(37)	
	4129					35					
Hγ	4340	45		57	37	57	51	25	53		
[O III]	4363					33	27	20		28	
He I	4471									6	
[Mg I]	4570	23								8	
	4615	29									
[Fe III]	4658	24								5	
He II	4686	(19)							10	2	
[Fe III]	4763	15									
Hβ	4861	100	100	100	100	100	100	100	100	100	100
[O III]	4959	11	62	108	95	150	125	73	51	88	96
[O III]	5007	50	180	342	286	449	390	235	206	270	255
[Fe II]	5159	15					10			8	
[N I]	5199						4			5	
Fe II]	5261	7					5				
[N II]	5755			12	4	17	8	4	6	7	
He I	5876		(16)		9	20	20	6	8	8	
	6030							3			
	6148							6			

Table 1 – *continued*

		1	2	3	4	5	6	7	8	9	10
[O I]	6300	149	87	70	61	51	72	83	68	69	58
[O I]	6364	45	32	27	24	14	23	22	10	23	18
[N II]	6548	70	77	84	77	68	83	72	51	65	84
Hα	6563	300	300	300	300	300	300	300	300	300	300
[N II]	6584	251	200	304	277	215	268	239	207	254	286
[S II]	6717	134	85	93	70	54	79	100	74	80	79
[S II]	6730	172	99	144	119	67	111	113	96	104	95
	6818					6					
	6828					7					
[O II]	7320			26	51				45	49	18
[O II]	7330			24	20						21
$F(\mathrm{H}\beta) \times 10^{14}$		1.40	0.74	1.47	2.60	1.38	6.4	1.97	0.64	2.71	0.72
c		0.86	0.90	0.96	0.79	0.86	0.76	0.87	1.02	0.65	0.06

Table 2. Dereddened emission line intensities for five positions in the SNR RCW 103.

	1	2	3	4	5
[O II] 3726		448	} 1460		} 1570
[O II] 3729		399			
H I 3835			43		
[Ne III] 3869			41		
H + He I 3888			(32)		
[S II] 4069			(27)		
[S II] 4076					
Hγ 4340		44	55		72
[O III] + [Fe II] 4363			24		26
[Fe III] 4658		10	11		9
He II 4686		4	5		
Hβ 4861	100	100	100	100	100
[O III] 4959	98	100	92	123	112
[O III] 5007	239	297	271	379	352
[Fe II] 5159	6	9	1		11
[N I] 5199	17	11	22		24
[Fe II] 5261		3	2		
[Fe III] 5270		4	4		7
[N II] 5755		4	8	7	9
He I 5876	17	12	15	10	10
[O I] 6300	89	73	116	85	126
[O I] 6364	19	21	32	36	39
[N II] 6548	138	151	189	162	163
Hα 6563	300	300	300	300	300
[N II] 6584	451	512	577	556	537
[S II] 6717	127	140	151	112	107
[S II] 6730	169	180	173	166	143
[O II] 7320	18			16	
[O II] 7330	25			38	
$10^{14} F(\mathrm{H}\beta)$	0.37	1.65	2.24	0.43	1.70
c	2.16	2.21	2.12	1.81	1.97

Table 3. Dereddened emission line intensities for six positions in Kepler's SNR.

		1	2	3	4	5	6	$f(\lambda)$
[O II]	3727	(700)		1100		700		0.33
[Ne III]	3868	70						0.28
Ca II	3933	(5)						0.26
[Ne III]	3968	24						0.25
	4018	(7)						0.24
[S II]	4069	125	97	142	94	133		0.22
[S II]	4076	34			33			0.22
[Fe III]	4250	(4)						0.17
	4308			9				0.15
Hγ	4340	40	37	48	20	33	18	0.15
[Fe II]	4359	(5)						0.14
[O III], [Fe II]	4363	20		27	12			0.14
[Fe II]	4413	9						0.13
	4607	(3)	12					0.07
	4615	(1)						0.07
[Fe III]	4658	11			11	6		0.06
He II	4686	(1)			6			0.05
Hβ	4861	100	100	100	100	100	100	0.00
[O III]	4959	79	36	63	76	87	30	−0.03
[O III]	5007	253	272	207	265	291	172	−0.04
[Fe II]	5159	25	(3)	17	25	12	5	−0.08
[N I]	5199	3	(7)	11	5	5		−0.09
[Fe II]	5261	10		13	7	4		−0.10
[Fe III]	5270	10		4	7	5		−0.11
	5281	(1)						−0.11
[Fe XIV]	5301	(1)						−0.11
	5338				(2)			−0.12
	5431	(<1)			(3)			−0.14
	5471	(1)						−0.15
	5491				(1)			−0.16
[Fe II]	5527	3			4			−0.16
[N II]	5755	15		20	19	9	5	−0.21
He I	5876	16		13	11	6	8	−0.23
	6066	(<1)						−0.27
	6083	(<1)						−0.27
	6239	(1)						−0.30
	6262	(1)						−0.30
	6277	(<1)						−0.30
[O I]	6300	115	84	142	139	111	65	−0.31
[Fe II]	6332		9					−0.31
[O I]	6364	35	19	42	43	30	19	−0.32
[N II]	6548	162	146	187	157	194	147	−0.35
Hα	6563	300	300	300	300	300	300	−0.35
[N II]	6584	532	467	582	543	626	450	−0.35
[S II]	6717	52	36	72	51	66	67	−0.37
[S II]	6730	102	80	141	104	142	110	−0.38
	6828	4		7		18		−0.39
	6861	(1)		3	4	3		−0.39
	6923	(1)						−0.40
	6971					1		−0.41
	6990	(<1)						−0.41
	7053			(2)				−0.42
	7113				3			−0.43
	7124					4		−0.43
	7141	29		25	29	18		−0.43

Table 3 – *continued*

		1	2	3	4	5	6	$f(\lambda)$
[Fe II]	7155	24		17	14	8	8	−0.43
	7244	(<1)		(17)	14	11		−0.44
[Fe II]	7288	(29)						−0.45
[O II]	7320	(50)						−0.45
[O II]	7330	(30)						−0.46
$F(H\beta)\times10^{14}$		1.32	0.32	0.80	0.87	1.12	0.53	
c		1.51	2.45	1.26	1.28	1.35	1.42	

Table 4. Dereddened emission line intensities in Galactic SNRs.

		RCW 86 (i)	RCW 103 (i)	Kepler (i)	Cygloop (ii)	Cas-A (Q) (iii)	Crab (iv)	IC 443 (v)	Vela (vi)	CTA 1 (vii)
[O II]	3727	>360	1210	(>700)	1383		1025	736		1242
[Ne III]	3869		(16)	21	68		115	35		
[S II]	4069	23	(9)	116	18		} 49	22	} 44	
[S II]	4076	4		21	6			4		
Hδ	4102	25			24		19	22	25	
Hγ	4340	44	50	36	47		47	47	52	
[O III] + [Fe II]	4363	17	16	14	36		15	7	53	
[Fe II]	4413			3						
He I	4471						14			
[Fe III]	4658	2	8	7			12		6	
He II	4686	2	3	1	5		44	3	2	
Hβ	4861	100	100	100	100	100	100	100	100	100
[O III]	4959	98	102	76	147	<58	249	42	185	256
[O III]	5007	303	305	253	439	43	783	130	575	833
[Fe II]	5159	4	9	17		33	4	6	3	
[N I]	5199	4	18	4			4	15	7	
[Fe II]	5261	2	2	9				2		
[Fe III]	5270	2	4	4			6	3		
[Fe II]	5527			2		14				
[N II]	5755	7	7	11	7	65	4	3	11	
He I	5876	11	12	12	8	32	46	8	6	
[O I]	6300	76	103	117	22	85	98	75	17	<204
[O I]	6364	24	30	35	7	27	32	25	5	
[N II]	6548	76	168	167		252	108	55	89	
Hα	6563	300	300	300	300	300	300	300	272	300
[N II]	6584	258	542	535	255	740	357	170	261	257
[S II]	6717	84	134	55	172	4	}390	181	127	221
[S II]	6730	115	168	112	138	13	419	148	115	174
	7140			13						
[Fe II]	7155			9		10	8			
[O II]	7320				} 55	} 22	} 25	} 27	} 57	} 159
[O II]	7330									
c		0.78	2.09	1.46	0.12	3.00	0.68	1.18	0.00	0.52

References
(i) This work.
(ii) Miller (1974).
(iii) Kirshner & Chevalier (1977) (quasi-stationary flocculi).
(iv) Fesen & Kirshner (1982).
(v) Fesen & Kirshner (1980).
(vi) Danziger & Goss (in preparation).
(vii) Fesen *et al.* (1981).

and $f(\lambda)$ is the reddening function (Osterbrock 1974). In the last column of Table 3 we give the values of $f(\lambda)$ that were used in our reddening correction. The tables also give the measured fluxes in Hβ at each position, in units of $10^{-14}\,\mathrm{erg\,cm^{-2}\,s^{-1}}$.

In Table 4 we present integrated spectra of our three SNRs. The lines include all of those that were identified in at least two different positions in one of the objects. The numbers given in the table were obtained in the following way: for each line a weighted sum of the intensities outside the Earth's atmosphere over all the observed points was taken. The weights are the absolute fluxes of Hβ measured at each point and given in Tables 1, 2 and 3. The spectrum of each source obtained in this way is a good approximation to the spectrum that would have been measured had the object been spatially unresolved, for example if the remnant was observed in an external galaxy. A reddening correction was then applied as in Tables 1, 2 and 3. A similar integration was performed over the observations for the other sources in Table 4, except for CTA 1 and Vela for which the intensities at only one position in the source are given. The reddening correction parameter for each nebula is also given in Table 4.

4 Discussion

4.1 INTERSTELLAR REDDENING

The interstellar reddening for all the points observed was estimated by assuming that the true, unreddened Hα/Hβ line ratio in all spectra has the value of 3 and by using the Galactic reddening law derived by Whitford (1958) and given by Osterbrock (1974). The value 3 for the Hα/Hβ ratio is consistent with a large range of shock models (Raymond 1979; Shull & McKee 1979). It approximates a representative value for this ratio in the radiative recombination theory for the hydrogen emission spectrum (Brocklehurst 1971), which is applicable in our cases. The shock velocities implied by a few observed line ratios that are insensitive to reddening are of the order of $100\,\mathrm{km\,s^{-1}}$ or larger (see below). In this velocity range, hydrogen in the pre-shock region is fully ionized by the UV radiation emanating from the hot region behind the shock front (Shull & McKee 1979; Dopita 1976). The error introducted by not considering variations in the Hα/Hβ ratio due to variations in the density and the temperature in the hydrogen recombination zone may reach 15 per cent in the relative intensity of red/blue lines that lie in the opposite extremes of the spectral range in our spectrograms.

4.2 GENERAL SPECTRAL CHARACTERISTICS

The spectra presented in Table 4 enable one to note a few characteristics of the overall spectra of the three SNRs in our program and to compare them with other Galactic remnants.

(1) A common characteristic of the three SNRs is the small value of the [S II] 6717/6730 line ratio, much less than 1, reaching in Kepler the lowest value of 0.49. This implies high densities in the S II regions, of the order of $10^3\,\mathrm{cm^{-3}}$. In Dopita's (1977) diagnostic diagrams, Kepler's SNR (for example) lies in the regime of a post-shock temperature $T_2 > 10^5$ K and a pre-shock density $N_1 > 10^3\,\mathrm{cm^{-1}}$.

(2) The He II λ4686 line is present in the spectra of the three remnants discussed here. General considerations of the physical conditions near a shock front (Osterbrock & Dufour 1973) and most of the published models (Raymond 1979; Shull & McKee 1979) imply that shock velocities of $\sim 100\,\mathrm{km\,s^{-1}}$ or higher are required to produce this line. Furthermore,

the observed O III/Hβ ratios in the three sources, taking the value 4.2 in RCW 86 and 103 and the value 3.4 in Kepler, are also consistent, according to the models, with shock velocities $\geqslant 100\,\mathrm{km\,s^{-1}}$.

(3) Kepler's SNR and RCW 103 have large [N II]/Hβ ratios of the order of 7, while in RCW 86 this ratio is ~ 3 (in our notation, a symbol of an ion in a line-intensity ratio represents the sum of all the lines of that ion observed in the spectrum). Daltabuit, D'Odorico & Sabbadin (1976) and D'Odorico & Sabbadin (1976) have noted in Galactic SNRs a correlation between the [N II]/Hα ratio and the density parameter [S II] 6717/6730 ratio, and also between the [N II]/Hα ratio and the diameter of remnants.

With the help of the intensities presented in Table 4, one is able to show that these correlations are due, at least partially, to an abundance effect of nitrogen. Consider, for example, Kepler's SNR with the high ratio of [N II]/Hβ = 7.13 on one hand and IC 443 with [N II]/Hβ = 2.28 on the other. We now compare the value of the ratio [O III]/[O I] = 2.26 in Kepler with the value 1.79 in IC 443. In the range of shock velocities $100 \leqslant v < 200\,\mathrm{km\,s^{-1}}$, the higher the value of the [O III]/[O I] parameter, the larger is the fraction of the O^{++} ionization zone; the singly-ionized species occupy a smaller region in the emitting filament. This effect is well demonstrated in models, E, F, G, H and I of Raymond (1979) and in models by Shull & McKee (1979). We therefore expect that, for equal relative abundances of nitrogen in the two remnants, the [N II] lines should be equal or even slightly more enhanced in IC 443 than in Kepler. The fact that Kepler is more dense than IC 443 as indicated by the value of the [S II] 6717/6730 ratio, which is 0.49 in Kepler and 1.20 in IC 443, tends to strengthen this expectation. The much larger [N II]/Hβ value in Kepler implies therefore a higher abundance of nitrogen in this nebula. We arrive at the same conclusion when we derive the abundance of nitrogen in the two remnants, using the formal procedure suggested by Dopita (1977). We obtain for Kepler an abundance of nitrogen relative to hydrogen of $\mathrm{N/H} \sim 13 \times 10^{-5}$, while in IC 443 the corresponding value is $\sim 3 \times 10^{-5}$.

(4) A few [Fe II] and [Fe III] lines have been measured in our three objects and their intensities are given in Table 4. The three SNRs, RCW 86, 103 and IC 443 have identical spectra of [Fe II]. The two latter remnants have also the same [Fe III] spectra whereas the lines of this species in RCW 86 are half as strong. Kepler's SNR has the same [Fe III] spectrum as RCW 103 and IC 443 but all the [Fe II] lines in its spectrum have about twice the intensity of the corresponding lines in the other three remnants. We may add that the iron spectrum of Kepler is virtually identical to that of the LMC SNR N49 (Osterbrock & Dufour 1973). In the spectrum of the Vela filament only two Fe lines have been measured. Their intensities are similar to those of the corresponding ones in RCW 103. In Cas A only [Fe II] lines are observed, in general much stronger than in all other objects. In the Crab nebula only the [Fe III] line at λ 4658 has been recorded.

All the differences in the relative intensities of the iron lines among the sources in Table 4 are probably compatible with a similar abundance of the element in each remnant and differences in the excitation conditions. A possible exception is RCW 86 that has both weak [Fe III] and weak [Fe II] lines. Since RCW 86 shows no sign of a particularly high excitation state relative to the other remnants in the table, as indicated for example by similarities in the [O III]/[O I], the [O III] 5007/4363 or the [N II] 6584/5755 ratios, it is unlikely that large quantities of iron are present in this nebula in higher ionization states. We therefore conclude that the abundance of iron in RCW 86 is lower than in RCW 103, Kepler and IC 443.

(5) The reddening that we have derived from RCW 86 corresponds to a visual extinction toward this object of $A_{\mathrm{v}} = 1.7$ mag. This value is in good agreement with Westerlund

(1969a), who has estimated $A_V = 2$ mag on the basis of an association of the SNR with OB stars. It is also in good agreement with the implied, though incorrectly stated, results obtained by Ruiz (1981) and the value implied by the measurements by Dopita, D'Odorico & Benvenuti (1980). RCW 86, at $l = 315°.4$, $b = 2°.3$, lies close to the Galactic plane but not in the direction of the Galactic centre. We can therefore use the mean value of the interstellar visual extinction to make a crude estimate of the distance to this object. With an average extinction per unit length in the Galactic plane of 0.8 mag/kpc and a scale height of absorption above the Galactic plane of 140 pc (Allen 1973) we obtain $d = 3.2$ kpc. This value coincides with the distance adopted by Clark & Caswell (1976) on the basis of the Σ–D relation.

The visual extinction to RCW 103 implied by our reddening value is $A_V = 4.5$ mag, whereas Dopita *et al.* (1980) obtain 3.8 mag, and Westerlund (1969b) 3 mag by the OB association method. The kinematic distance derived from radial velocities of radio 21-cm and OH lines is 3.2 kpc (Caswell *et al.* 1975; Caswell & Robinson 1974), but Clark & Caswell (1976) adopt $d = 8.7$ kpc on the basis of the Σ–D relation. The extinction distance that can be derived from our value of A_V is 6.6 kpc.

The distance to Kepler has been discussed by Danziger & Goss (1980) and is based in part on reddening derived with the spectrophotometric data discussed here. That estimate of the visual absorption, $A_V = 3.5$, remains the most direct one in a part of the sky that has patchy obscuration. A distance of 3.2 kpc implied by that value in conjunction with a rediscussion of historical data remains the most attractive.

4.3 DETAILED SPECTROSCOPY

4.3.1 *RCW 86*

From the values of the reddening parameter c given in Table 1 we see that the extinction varies across the image of the nebula. Part of the apparent variation is due to the observational errors in the value of the $H\alpha/H\beta$ ratio, and to differences between true values of this ratio and the assumed one of three. These, however, cannot account for the entire range of the c-values, in particular for the outstanding value of 0.06 in point 10. It seems that at this position we have been observing the nebulosity through a hole in the foreground absorbing interstellar matter. van den Bergh (1971) has suggested that such holes are present in the foreground of the Cas A SNR.

We observe in Table 1 that some of the major spectral line intensities vary considerably from point to point. For example in point 1 we find $[O\,\text{III}]/H\beta = 0.6$ as compared to 6 in point 5. The $[N\,\text{II}]/H\beta$ and the $[S\,\text{II}]/H\beta$ ratios are much more uniform across the remnant. These observations at present lack a detailed physical understanding. In all points $6717/6730 < 1$, indicating, according to Dopita's (1977) and other models, a pre-shock density larger than $100\ \text{cm}^{-3}$.

The important lines of $[O\,\text{II}]$ at $\lambda 3727$ have not been observed by us in RCW 86, so a direct estimate of the abundances in the filaments seems to be impossible. We also find that all the observed values of the $[O\,\text{III}]\,5007/[O\,\text{I}]\,6300$ ratio, except at points 1 and 2, fall outside the range of shock conditions considered by Dopita (1977).

Among the published models of SNRs heated by shocks, there are only a few with large pre-shock densities and large shock velocities. It seems that model H of Shull & McKee (1979) may roughly represent the filaments observed in our points 3–10. This model assumed a shock velocity of $100\ \text{km s}^{-1}$ and a pre-shock density of $100\ \text{cm}^{-3}$.

The spectrum of point 1 in RCW 86 is more difficult to understand. At this point the $[S\,\text{II}]$ density parameter 6717/6730 as well as the $[N\,\text{II}]/H\beta$ ratio have values similar to those at the other points, but the [O III]/Hβ ratio is significantly smaller. According to all models, such a small [O III]/Hβ ratio is expected at low shock-velocities.

The spectrum of RCW 86 by Dopita *et al.* (1980) is quite similar to our spectrum at point 7 except that our blue [S II] lines have twice the intensity measured by Dopita *et al.*

There are some differences between our relative line strengths and those published by Ruiz (1981). Many of our points lie outside the brightest parts of the filaments, which may explain why our [S II] line strengths are on average lower. One point almost in common to the two studies (our position 3, Ruiz position A) shows reasonable agreement, although the Ruiz Balmer decrement appears anomalous. Her conclusion, that variations in the [N II]/Hα ratio imply variations in abundance of nitrogen, may be premature in view of our observed variations of the electron temperature implied by variations in the [N II] 5755/6584 ratio.

4.3.2 RCW 103

This SNR was also recently observed by Dopita *et al.* (1980). Since they used a long slit in their measurements, a comparison of their measurements might be made with our integrated spectrum. Inspection of Table 4 of this paper and table 1(c) of Dopita *et al.* shows that the two spectra are indeed similar. Dopita *et al.* have analysed in great detail the spectrum of RCW 103 and have derived the abundances of elements in this nebula, along with many others. In view of the similarity of their spectrum to most of ours, their analysis is applicable to our spectra.

We have one observational point in the northern wisp of RCW 103, namely point 1, while the other four are in the southern, major nebulosity of this remnant (see Plate 2). Point 1 is also slightly peculiar in its spectrum. Inspection of Table 3 reveals that both the [O III] and the [N II] lines are significantly fainter than in the southern nebula. The lack of measurements of the [O II] λ3727 doublet at this point makes it difficult to determine the physical nature of their differences.

RCW 103 deserves further attention in view of the recent discovery of a compact X-ray source in its centre (Tuohy & Garmire 1980). If this source is indeed a pulsar or a hot neutron star at the centre of the gaseous remnant, one might expect, in analogy with the Crab SNR, that radiation from the vicinity of the neutron star is also contributing to the excitation of the nebula, or at least to the parts immediately surrounding the neutron star.

4.3.3 Kepler

Three of our six observational points in Kepler's SNR can be identified to a good approximation with three of the knots of van den Bergh & Kamper (1977). A comparison of Plate 3 with fig. 2 of these authors shows that our point 1 is in knot 26, point 3 is in knot 3 and point 4 in knot 7. Minkowski (1959) has measured a radial velocity of $-180\,\mathrm{km\,s^{-1}}$ in knot 26.

In Table 3 we see that the interstellar extinction is varying from point to point in the Kepler SNR. Here again, part of this variation is probably due to the observational errors in the line intensities and to variations in the intrinsic value of the Hα/Hβ ratio. Some of these variations are real, however, particularly in the outstanding point 2. The aperture position at this point is only a few arcsec south of position 1, yet the difference in the derived visual extinction to these two points is 2 mag. Although the Kepler SNR is in a region of strongly varying obscuration, evident on SRC Schmidt plates, it seems that the outstanding extinction towards point 2 is associated with local conditions. Furthermore, van den Bergh & Kamper (1977) have found that among all non-crowded field stars with $V < 16.0$ and

$B < 14.0$ within 10 arcmin of Kepler's SNR, the maximum reddening is $E(B-V) = 0.9$. The sharp gradient in the extinction over an angular separation of a few arcsec may indicate that point 2 in Kepler is seen through a cold, dark inhomogeneity or cloudlet in the vicinity of the emitting remnant. Such cloudy interstellar matter was proposed by McKee & Cowie (1975) and others as the medium in which the blast wave of a supernova explosion appears as the observable optical and X-ray SNRs. In fact, with a few general assumptions, we may obtain an estimate to the dimensions of the cloudlet that obscures point 2. We assume that $\Delta c \sim 1$, and that the difference between the reddening to point 2 and the general reddening to the remnant is due to absorption in the cloudlet. The extinction in magnitude of light transmitted through an absorbing medium of length D_a is $A = 1.086\, N_g \sigma D_a$, where N_g is the density of the scattering or the absorbing particles and σ is the extinction cross-section. We write $N_g = \gamma N$, where N is the density of gas particles in the absorbing cloud and γ is the dust-to-gas ratio (by number) in the medium. We therefore have $D_a = A/1.086\,\gamma N \sigma$. Assuming that the grains in the cloudlet have the general average properties of dust in the Galaxy, we take from Allen (1973) $\gamma = 7 \times 10^{-13}$ and $\sigma \simeq 10^{-9}$. The visual extinction *in the cloudlets* is $A = 2$ mag, hence $D_a = 850/N$ pc. Taking for the pre-shock density the value $N = 10^3$ (see below), we obtain $D_a = 0.85$ pc.

The absorbing material responsible for $\Delta c = 1$ in point 2 can also be the near end of the interstellar inhomogeneity, whose far side is now being heated by an approaching shock, giving rise to the observed spectrum in this point. For an assumed velocity of $100\,\mathrm{km\,s^{-1}}$ it will take ~ 8000 yr for the shock to 'eat' its way through the dark cloud.

The interpretation of the spectrum of point 2 as the emission from a plasma heated by a shock front that is viewed faced-on can also be applied to the observed Hβ flux F. This gives consistent results with other known parameters of the remnant. For we can write expressions for F for two limiting cases:

(i) A shock with a single recombination event per emitting hydrogen atom.
(ii) A shock with multi-recombination events.

In case (i), each hydrogen atom in the emitting filament undergoes one recombination event that gives rise to a transition into the $n = 2$ energy level of the atom, with the emission of one Balmer photon. In this case N_B, the number of Balmer photons emitted per second, is equal to the number of hydrogen atoms that are passing in one second through the shock front or through the fore-running ionization front (we thank the referee for bringing this point to our attention). Therefore $N_B = N_H S v$, where $N_H = N$ is the pre-shock density (of hydrogen atoms), S is the area of the shock front (in a plane parallel approximation) and v is the shock velocity. From radiative recombination theory (Brocklehurst 1971), the number of emitted Hβ photons is $N_\beta = \eta N_B$, where $\eta \sim 1/6$.

The Hβ luminosity of the filament is $L_\beta = \eta N_B h\nu_\beta$. The entrance aperture of our spectrograph defines a surface area s at the source that is emitting into our instrument. Since we are viewing the shock front face-on, s is a fraction of the shock-front area S. The observed Hβ flux is therefore $F = (s/S)(L_\beta/d^2)10^{-c}$, where d is the distance to the remnant and c is the reddening value toward point 2, given in Table 3. Since $s = d^2\Omega$, where Ω is the solid angle defined by our entrance slot ($3.5 \times 3.5\ \mathrm{arcsec}^2$), we have $N_H = 10^c F/\eta\Omega v h\nu_\beta$. With the assumed velocity $v = 100\,\mathrm{km\,s^{-1}}$, we obtain $N_H \sim 1600\,\mathrm{cm^{-3}}$. This result is in excellent agreement with the estimate of the pre-shock density based on line intensity ratios and the use of Dopita's (1977) diagnostic diagrams (see below).

In case (ii), each hydrogen atom in the emitting filament undergoes more than one transition into the $n = 2$ energy level. These multi-recombinations follow ionizations that are due either to collisions in the hot plasma or to the UV radiation field emanating from the shock region. The first possibility is admittedly inconsistent with our assumption (Section 4.1) regarding the radiative nature of the hydrogen spectrum. If this possibility prevails in point 2, the reddening correction we have applied is an overestimate. Most of our discussion regarding this point remains unchanged, however. The second possibility is clearly consistent with Section 4.1.

While, in case (i), most of the Balmer emission comes from a rather narrow hydrogen-recombination zone in the filament, in case (ii) we observe hydrogen radiation from the entire H II region. We can therefore use F, the observed flux in Hβ, for estimating the value of D_e, the dimension of the radiating plasma along the line-of-sight. The observed flux is

$$F = \frac{\alpha_\beta N_e^2 V}{4\pi d^2} \times 10^{-c},$$

where α_β is an effective recombination rate (in energy units) for the emission of the Hβ line, and V is the emitting volume, $V = d^2 \Omega D_e$.

We are assuming a filling factor $f = 1$ in the volume radiating into our entrance aperture. We have

$$D_e = 10^c \times \frac{4\pi F}{\alpha_\beta \Omega} \times \frac{1}{N_e^2}.$$

From Osterbrock (1974) we take $\alpha_\beta = 10^{-25}$ erg cm^3 s^{-1}. This is the value of the effective recombination rate in the density range of 10^2–10^6 cm^{-3} and at a temperature of $(1–1.5) \times 10^4$ K. We thus find

$$D_e = \frac{4.5 \times 10^5}{N_e^2} \text{ pc.}$$

Taking $N_e = 5 \times 10^3$ from our [S II] observations, we have $D_e = 0.02$ pc. This value is not in conflict with the computed extension of the H II region in models of shock-heated SNRs (see, for example, Dopita 1977).

If the material behind the advancing front has not had the time to recombine, the value of D_e is the depth into the cloud that has been reached by the shock since it started to interact with the cloud. This would imply that the cloud was first hit by the shock about 200 years ago. Considering the roughness of our assumptions this is in very good agreement with the known age of Kepler's SNR.

The picture is not inconsistent with the discovery by van den Bergh & Kamper (1977) of the brightening of a few emission flocculi in Kepler's SNR in the last 35 years. We draw attention to the fact that all the recorded changes are in the sense of increasing brightness – 'no flocculi have faded'. Considering now the intrinsic line-intensities in the filaments of Kepler, we first note the very low value of the [S II] 6717/6730 line ratio. The lowest value 0.45 belongs to point 2, but all the other points have a value near 0.5 or less, except point 6 with a value of 0.61. This difference is significant, being much larger than the uncertainties in this line ratio. It implies that at point 6 the density is about one half of the density in the other observed points.

Using Pradhan's (1978) collision parameters for the ground configuration of S II and Osterbrock's (1974) transition probabilities, we find that [S II] $I(6717)/I(6730) = 0.5$ implies $N_e/(T_e)^{1/2} = 45$, where N_e is the electron density and T_e is the electron temperature in the S$^+$ zone. This value of the [S II] line ratio hardly fits into the range of the parameters considered by Dopita (1977). His diagrams imply a pre-shock density > 10^3 cm^{-3} and a post-shock temperature $> 10^5$ K. In fact, according to Dopita's diagrams the value 0.51 of the [S II] density ratio in point 3, for example, is irreconcilable with the value of $I(5007)/I(3727) = 0.2$ measured at the same point.

So far, to our knowledge, no model for SNR has been published which yields a value of the 6717/6730 ratio as low as observed in Kepler. The closest is model FF of Raymond (1979) which has 0.58 for this parameter. Model FF in any case cannot represent the observed spectra in Kepler since it is in disagreement with other important observed line ratios such as [O III]/Hβ or [S II] 4070/Hβ. Another characteristic of the observed spectra of Kepler is the ratio [N II] 6584/[O III] 5007 which has high values, mostly > 2. High values of this ratio are easily reached at low shock velocities, when the energy transferred into heat at the shock front is not enough to maintain a large O^{++} zone. For reasons discussed in Section 4.2, however, we believe that an abundance effect is indicated. Indeed, if one examines the [N II]/Hα ratios in all the SNRs in Table 4, one sees a tendency for smaller (younger) remnants to have stronger [N II] lines. This may be an abundance effect resulting from nitrogen-enriched material, ejected before (as quiescent mass loss) or during the explosion, being diluted with swept-up interstellar material.

A proper analysis of the spectra of the filaments in Kepler's SNR and the derivation of the abundances of the elements in this nebula must await the computation of models that include the range of line intensities and ratios presented in Table 3. Meanwhile it is instructive to compare the spectrum of Kepler with the spectra of Herbig–Haro objects obtained by Dopita (1978) and successfully compared with his models. We see that HHI and his Model 1 suggest that a model for Kepler might be possible with a high pre-shock density ($\gtrsim 200$–$300\,\mathrm{cm^{-3}}$), an increased nitrogen abundance ($\times 3.5$) and an increased shock velocity ($> 110\,\mathrm{km\,s^{-1}}$) to produce the strong [O III] lines.

5 Conclusions

Spectra of a few different regions in the three Galactic SNRs RCW 86, 103 and Kepler have been presented. All three objects are characterized by large electron densities in the emitting regions, of the order of $10^3\,\mathrm{cm^{-3}}$. They all have, in most of the observed points, intense emission lines of [O III] and [N II]. In all three objects the interstellar or the circumstellar extinction varies from point to point in the nebula, particularly in RCW 86 and in Kepler. These two sources exhibit also significant variations in their spectral appearance in different points.

We believe that the data presented in Tables 1, 2 and 3 may serve to test theoretical models of SNR filaments. In particular it is interesting to know whether the spectral variations observed in RCW 86 and in Kepler can be interpreted as resulting from variations in shock velocities alone, or whether they indicate variations in the chemical composition or other physical parameters in one and the same remnant.

Acknowledgments

EML thanks ESO for its hospitality and Dr M. Contini for some very useful discussions and contributions to this work.

References

Allen, C. W., 1973. *Astrophysical Quantities*, 3rd edn., Athlone Press, London.
Blair, W. P., Kirshner, R. P. & Chevalier, R. A., 1981. *Astrophys. J.*, **247**, 879.
Brocklehurst, M., 1971. *Mon. Not. R. astr. Soc.*, **153**, 471.

Bychkov, K. V. & Pikel'ner, S. B., 1975. *Soviet Astr. Lett.*, **1**, 14.
Caswell, J. J. & Robinson, B. J., 1974. *Aust. J. Phys.*, **27**, 597.
Caswell, J. L., Murray, J. D., Roger, R. S., Cole, D. J. & Cooke, D. J., 1975. *Astr. Astrophys.*, **45**, 239.
Clark, D. H. & Caswell, J. L., 1976. *Mon. Not. R. astr. Soc.*, **174**, 267.
Daltabuit, E., D'Odorico, S. & Sabbadin, F., 1976. *Astr. Astrophys.*, **52**, 93.
Danziger, I. J. & Dennefield, M., 1976. *Publ. astr. Soc. Pacific*, **88**, 44.
Danziger, I. J. & Goss, W. M., 1980. *Mon. Not. R. astr. Soc.*, **190**, 47P.
D'Odorico, S. & Sabbadin, F., 1976. *Astr. Astrophys.*, **50**, 315.
D'Odorico, S. & Sabbadin, F., 1977. *Astrophys. J. Suppl.*, **28**, 439.
Dopita, M. A., 1976. *Astrophys. J.*, **209**, 395.
Dopita, M. A., 1977. *Astrophys. J. Suppl.*, **33**, 437.
Dopita, M. A., 1978. *Astrophys. J. Suppl.*, **37**, 117.
Dopita, M. A., D'Odorico, S. & Benvenuti, P., 1980. *Astrophys. J.*, **236**, 628.
Dopita, M. A., Mathewson, D. S. & Ford, V. L., 1977. *Astrophys. J.*, **214**, 179.
Fesen, R. A. & Kirshner, R. P., 1980. *Astrophys. J.*, **242**, 1023.
Fesen, R. A. & Kirshner, R. P., 1982. *Astrophys. J.*, **258**, 1.
Fesen, R. A., Blair, W. P., Kirshner, R. P., Gull, T. R. & Parker, R. A. R., 1981. *Astrophys. J.*, **247**, 148.
Kirshner, R. P. & Chevalier, R. A., 1977. *Astrophys. J.*, **218**, 142.
McKee, C. F. & Cowie, L. L., 1975. *Astrophys. J.*, **195**, 715.
Miller, J. S., 1974. *Astrophys. J.*, **189**, 239.
Minkowski, R., 1959. *Paris Symposium on Radio Astronomy*, p. 315, ed. Bracewell, R. C., Stanford University Press.
Oke, J. B., 1974. *Astrophys. J. Suppl.*, **27**, 21.
Osterbrock, D. E., 1974. *Astrophysics of Gaseous Nebulae*, Freeman, San Francisco.
Osterbrock, D. E. & Dufour, R. J., 1973. *Astrophys. J.*, **185**, 441.
Pradhan, A. K., 1978. *Mon. Not. R. astr. Soc.*, **184**, 89P.
Raymond, J. C., 1979. *Astrophys. J. Suppl.*, **39**, 1.
Ruiz, M. T., 1981. *Astrophys. J.*, **243**, 814.
Shull, J. M. & McKee, C. F., 1979. *Astrophys. J.*, **227**, 131.
Tuohy, I. & Garmire, G., 1980. *Astrophys. J.*, **239**, L110.
van den Bergh, S., 1971. *Astrophys. J.*, **165**, 457.
van den Bergh, S. & Kamper, K. W., 1977. *Astrophys. J.*, **218**, 617.
van den Bergh, S., Marscher, A. P. & Terzian, Y., 1973. *Astrophys. J. Suppl.*, **28**, 19.
Westerlund, B. E., 1969a. *Astr. J.*, **74**, 879.
Westerlund, B. E., 1969b. *Astr. J.*, 74, 882.
Whitford, A. E., 1958. *Astr. J.*, **63**, 201.